Journal of Engineering Science and Technology Review 15 (5) (2022) 62 - 69

JOURNAL OF
Engineering Science and Technology Review

www.jestr.org

Research Article

Numerical Simulation on Creep Properties of Cutting Loess Slope under Influences of Long-term Rainfall

Peng He[1,*] and Lei Ge[2]

[1]Shaanxi Water Group Water Ecology Comprehensive Development Co., Ltd, Shaanxi, 710018, China
[2] Shaanxi Transportation Holding Group Co., Ltd., Xi'an 710065, China

Received 30 May 2022; Accepted 19 November 2022

Abstract

Cutting is a common governance method of loess slope, and it has been widely applied worldwide. However, cutting loess slopes develop abundant instability failure under influences of rainfall. Studies on creep failure mechanism of loess slope under influences of long-term rainfall are insufficient. To disclose the creep failure mechanism of loess slope under influences of rainfall, a fluid–solid coupling computation of a typical cutting loess slope in Loess Plateau in Shaanxi Province of China was conducted based on the Burgers creep model by using ABAQUS software. The internal mechanical mechanism of loess slope failure caused by rainfall was analyzed according to calculated changes in pore water pressure, shear stress, equivalent plastic strain, and displacement of critical point. Results show that great excess pore water pressures at different-level slope shoulder are the primary cause of rainfall-induced landslide of loess slope. Rainfall cuts shoulders of loess slope, and the overall shape of slope surface is arc-like. Deformation failure of cutting loess slope under influences of rainfall is the retrogressive failure which develops gradually upward from level-1 slope foot. Slow creep is observed in shear stress at the slope foot and horizontal displacements at different-level slope shoulders. However, creep rate decreases gradually, and it is not the primary cause of instability failure of the loess slope. The proposed creep failure mechanism of loess slope under influences of rainfall deepens understanding on stability development of loess slope. It could be used in the practical engineering to evaluate the development stage of loess slope stability under influences of rainfall.

Keywords: loess slope, cutting, creep, rainfall infiltration, stability

1. Introduction

Loess is the yellow loose stacking material formed in Quaternary and extensively distributed in continents around the world. Its distribution is discontinuous at middle-latitude zones of Southern and Northern Hemispheres from east to west, and it accounts for about 1/10 of total area in the world [1]. China is the country with the most extensive and thickest distribution of loess in the world. In particular, loess is extensively distributed in Northwest China, and it accounts for 3.96% of China’s territory. Loess brings some challenges to engineering construction due to its unique mechanical properties [2][3]. Since China launched the China Western Development program, several infrastructures have been built in Northwest China, including industrial and civil projects, highway and bridge projects, and water conservancy facilities [4][5]. Thus, developing several loess slope governance projects is inevitable. Cutting treatment has been widely applied in loess slope governance due to its simple construction, high economic efficiency, and good effect [6]. However, engineers in governance engineering design often consider the current stability only, but they ignore deformation failure of loess slope under influences of long-term rainfall due to technological or economic reasons. As a result, several cutting loess slopes may develop the secondary disasters [7]. Thus, studying the deformation failure mechanism of cutting loess slope under influences of long-term rainfall is extremely important.

Loess slope is extremely easy to be failed under influences of rainfall due to the unique water sensitivity of loess. Collapse, dislocation, large deep gully, and ponor are typical failure modes of cutting loess slope [8]. With respect to internal causes of failure, on the one hand, internal structural failure occurs as a response to rainfall due to strong water sensitivity of loess [9][10]. On the other hand, failure of cutting loess slope is caused by creep of loess under influences of long-term rainfall. The loess slope surely may be collapsed after long-term accumulation of creep deformation [11]. Thus, deformation failure mechanism of loess slope should be discussed from the perspective of loess creep.

The development of engineering technology has facilitated the use of computer simulation technology in the analysis of slope stability and deformation failure. It includes finite element, finite interpolation, and discrete element analysis theories. Different boundary conditions could be set to the solving equation by using these theories to simulate different rainfall conditions. As a result, some deformation failure laws of slope under rainfall conditions are formed, such as slope surface erosion development laws [12], occurrence laws of slope landslide [13], and slope collapse laws [14]. These laws can provide some guidance to slope disaster control. However, the research conclusions above still have some limitations. On the one hand, they only considered short-term rainfall conditions but cannot discuss influences of rainfall cycles over years during operation. On the other hand, they ignored influences of

*E-mail address: 3020581746@qq.com

doi:10.25103/jestr.155.09

long-term creep of loess on deformation failure. Therefore, loess slope under long-term operation after governance still has to be further analyzed to disclose the deformation failure mechanism.

In this study, a numerical simulation on creep performances of cutting loess slope under influences of long-term rainfall was conducted to analyze creep failure mechanism and provide guidance to engineering design of loess slope.

2. State of the art

Research methods of slope deformation failure mechanism mainly include model experiment, numerical simulation, and field monitoring [15][16]. Many scholars have studied failure mechanism of soil slope under influences of rainfall by using model experiment, which mainly concentrates on deformation development process of loess slope under influences of rainfall. Cogan et al. [17] studied rainfall-induced instability laws of soil slope by model experiment and found that soil slope developed instability failure when pore water pressure in slope reached the maximum or water content in slope reached a balance. Moreover, the instability developed earlier with the increase in initial water content, and the earliest instability failure occurred when the slope angle was 45°. Acharya et al. [18] investigated scoring and instability behaviors of loess slope by rainfall through a model experiment and found that erosion quantity increased significantly when landslide occurred at near slope edges. Moreover, the upper slope went down by scoring, while the lower slope degree decreased. Instability failure of loess slope under rainfall influences was progressive pull-type landslide. Derbyshire et al. [19] studied instability mechanism of loess slope by using model experiment and found that most instability failures of loess slope were progressive failures produced by tensile fractures. This condition was caused by decreasing shear strength of loess when internal structure of loess was lost because of the increasing water content. Chinkulkijniwat et al. [20] gained hydrogeological conditions in soil slope under rainfall influences through a model experiment. Stability changes of soil slope under rainfall influences were studied through theoretical calculation. The results showed that rainfall intensity influenced depth of slip surface seriously, and such influences weakened with the increase in cohesiveness of slope soil mass. In a word, existing associated research results mainly disclosed deformation failure process of soil slope, and they only considered influences of short-term rainfall. Moreover, internal mechanical evolution mechanism that causes slope instability under influences of rainfall has not been formed yet.

Researchers have analyzed deformation failure of loess slope under influences of long-term rainfall through numerical simulation to further disclose the mechanical evolution mechanism. Finite element analysis and finite interpolation analysis were commonly applied methods. Schwarber et al. [21] studied instability mechanism of loess slope under rainfall influences through numerical simulation and found that loess slope developed landslide instability. Instability of loess slope was influenced slightly by cohesiveness and internal friction angle of soil mass. Leshchinsky et al. [22] analyzed instability mechanism of loess slope under the collaborative influences of slope foot excavation and continuous rainfall through finite element method. They found that failure of loess slope was caused by the superficial landslide at slope foot, and it was induced by slope foot extraction. Cross [23] studied sensitivity of superficial soil slope stability to soil properties under rainfall influences through numerical calculation. The results showed that stability coefficient of slope was very sensitive to cohesiveness (c), water level in slope, and dip angle of slope. However, it was insensitive to internal friction angle and soil mass. Sadovenko [24] analyzed the deformation failure mechanism of loess slope under rainfall conditions by finite element method. The results showed that superficial soil mass saturated due to rainfall, which caused landslide. Shear deformation in slope loess was controlled by migration of wet peak and water content changes in soil mass. Chang et al. [25] proposed an improved finite element method to analyze instability mechanism of fractured loess slope. They found that fractures in loess slope propagated vertically in early stage of instability deformation development. Existing research results have well disclosed mechanical mechanism of deformation failure of loess slope, but creep factors of loess are ignored in numerical simulation. Thus, none of them can disclose creep mechanical mechanism of loess slope in long-term operation effectively.

Clearly, existing studies concerning influences of rainfall on loess slope mainly focus on deformation failure mechanism of slopes. They disclose the occurrence mechanism, development process, causes, and influencing factors of rainfall-induced loess landslide through experiments and numerical simulation. However, no numerical simulation results concerning influences of loess creep behaviors are available yet. Moreover, no report is available on creep process of cutting loess slope governance project under influences of long-term rainfall. Thus, the finite element software for typical cutting loess slope in northern Shaanxi Province, China was developed using the creep model and then used to analyze deformation failure mechanism of cutting loess slope under influences of long-term rainfall. It could provide some guidance to loess slope governance.

The remainder of the study is organized as follows. Section 3 elaborates the creep theory of loess and determination method of parameters, slope prototype characteristics, and major parameters for numerical modeling, numerical model, and calculation scheme. Section 4 introduces numerical calculation results, mainly including seepage, stress, and deformation calculation results. Moreover, creep failure mechanism of loess slope under influences of long-term rainfall is discussed according to the calculation results. Section 5 summarizes the conclusions.

3. Methodology

3.1 Creep theory of loess

Rheology is defined mechanically as the relationships of material stress and strain with time. Rheology of loess refers to creep [26][27]. Scholars proposed multi-element models to describe creep properties of loess, such as Maxwell, Kelvin, and Burgers models. Burgers model, which is suitable to loess, is widely used to describe creep of loess because it has explicit concept and few parameters that are easy to be determined [28].

Burgers model is formed by series connection of a Kelvin object and a Maxwell object (Fig. 1). It has four parameters (E_K, E_M, η_K, and η_M), where K refers to the Kelvin object and M refers to the Maxwell object. The creep equation of the Maxwell object can be expressed as

$$\varepsilon = \frac{\sigma}{E_M} + \frac{\sigma}{\eta_M} t \tag{1}$$

where E_M and η_M are modulus of compressibility and viscosity coefficient of the Maxwell object, respectively. Notably, E_M has to be transformed into the shear modulus (G_M) when describing shear rheology.

The creep equation of the Kelvin object is

$$\varepsilon=\varepsilon_0 \exp\left(-\frac{E_K}{\eta_K} t\right) + \frac{\sigma}{E_K}\left[1-\exp\left(-\frac{E_K}{\eta_K} t\right)\right] \tag{2}$$

where E_K and η_K are modulus of compressibility and viscosity coefficient of the Kelvin object, respectively. Similarly, E_K has to be transformed into the shear modulus (G_K) when describing shear rheology. ε_0 denotes the initial strain, and it is 0 in this study. Thus, Eq. (2) can be simplified as

$$\varepsilon=\frac{\sigma}{E_K}\left[1-\exp\left(-\frac{E_K}{\eta_K} t\right)\right] \tag{3}$$

Given that Burgers model is formed by series connection of a Maxwell object and a Kelvin object (Fig.1), strain of Burgers model shall be the sum of strains of the Maxwell and Kelvin objects. In this way, creep equation of the Burgers model can be obtained (Eq. (4)).

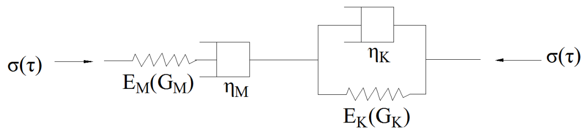

Fig.1. Burgers model

$$\varepsilon(t) = \sigma\left[\frac{1}{E_M} + \frac{t}{\eta_M} + \frac{1}{E_K}\left(1-e^{-\frac{E_K}{\eta_K}t}\right)\right] \tag{4}$$

where η_M and η_K are viscosity coefficients of the Maxwell and Kelvin objects, respectively. E_M and E_K are modulus of compressibility of the Maxwell and Kelvin objects, which have to be transformed into their shear modulus (G_M and G_K) when describing shear rheology. Thus, the shear rheology equation of the Burgers model can be obtained as

$$\varepsilon(t) = \sigma\left[\frac{1}{G_M} + \frac{t}{\eta_M} + \frac{1}{G_K}\left(1-e^{-\frac{G_K}{\eta_K}t}\right)\right] \tag{5}$$

3.2 Project background

The slope project in this study is located in Luochuan County, Yan'an City, Shaanxi Province (35°45'19.46"N, 109°25'34.63"E). It is a cutting loess slope and developed large-scaled collapse at the fifth year (Fig. 2). The average elevation of Luochuan County is about 1100 m, and it belongs to the temperate continental monsoon climate. The annual average temperature is 5–17 ℃, and the annual maximum temperature is 37.4 ℃. The annual average precipitation in Luochuan County is about 606 mm, and most rainfalls concentrate in July, August, and September.

Fig. 2. Slope prototype

It is a homogenous loess slope and has slopes composed of Epipleistocene (Q3) loess. The slope height is 17.6 m, and three-level cutting treatment is adopted. The level-1, level-2, and level-3 slope heights are 5, 4, and 5.6 m, respectively. Slope angles of all three levels are all 56°, and the platform width is 3.8 m.

3.3 Material parameters

Eq. (4) has to be transformed to some extent to acquire parameters of the Burgers model through a triaxial rheological experiment. The transformed Burgers model is expressed as follows:

$$\varepsilon(t) = A + Bt + C\left(1-e^{-Dt}\right) \tag{6}$$

Obviously, $A=\frac{\sigma_0}{E_M}$, $B=\frac{\sigma_0}{\eta_M}$, $C=\frac{\sigma_0}{E_K}$, $D=\frac{\sigma_0}{C\eta_K}$.

Next, time t is chosen as the arithmetic sequence by using tr as the tolerance, and ε is used to express strain. Let $X=\varepsilon(t+t_r)-\varepsilon(t)$ and $Y=\varepsilon(t+2t_r)-\varepsilon(t)$. Then, a linear relationship exists in Y–X:

$$Y = EX + F \tag{7}$$

Later, linear fitting is performed according to the triaxial rheological experimental data. Thus, E and F are obtained. Furthermore, B and D can be derived.

$$B=\frac{F}{t_r(2-E)},\ D=\frac{\ln(E-1)}{-t_r} \tag{8}$$

To calculate A and C, let $u=\varepsilon(t)-Bt$ and $v=1-e^{-Dt}$. In this way, Eq. (6) can be transformed as

$$u = Cv + A \tag{9}$$

Next, the u–v relation map is fitted according to triaxial rheological experiment. It is a straight, with a slope of C and an intercept of A. Finally, E_M, E_K, η_M, and η_K are converted from A, B, C, and D, respectively. The Burgers model parameters obtained in this study are as follows: E_M=80.6 kPa, E_K=109.7 kPa, η_M=237.0 kPa·day, and η_K=50.2 kPa·day.

Linear elastic model also is chosen in the elastic stage and the Mohr–Coulomb model is chosen in the plastic stage with considerations to the coupling analysis of rainfall influenced elastic-plastic stress and strain with seepage. The used material parameters are listed in Table 1. The elasticity modulus is tested by a confined compression test. *C* and *φ* in the Mohr–Coulomb model are tested by the direct shear test. Instruments and devices are shown in Fig. 3.

(a)

(b)

Fig. 3. Indoor experimental apparatus. (a) Confined compression apparatus. (b) Direct shear apparatus

Table. 1. Key material parameters

Name of parameters	Parameter values	Name of parameters	Parameter values
Humidity and density (g/cm3)	1.42	Modulus of compressibility (MPa)	5.58
Water content (%)	17.4	Internal friction angle (°)	27.0
Permeability coefficient (cm/s)	5.4×10^{-4}	Cohesive force (kPa)	15.0
E_M (kPa)	80.6	η_M (kPa·d)	237.0
E_K (kPa)	109.7	η_K (kPa·d)	50.2

3.4 Numerical model

In this study, the commercial software ABAQUS was developed for the second time using Burgers creep model. On this basis, the finite element model of slope was established. The quadrangle four-node fluid–solid coupling unit was applied for profiling. A total of 266 units were divided (Fig. 4). The boundary condition of complete constraint displacement was applied at bottom of the slope. The boundary condition of constrained horizontal displacement was applied on the right and rainfall flow was applied onto the slope surface according to practical situation. Rainfall flow shall be the rainfall intensity which changes with time.

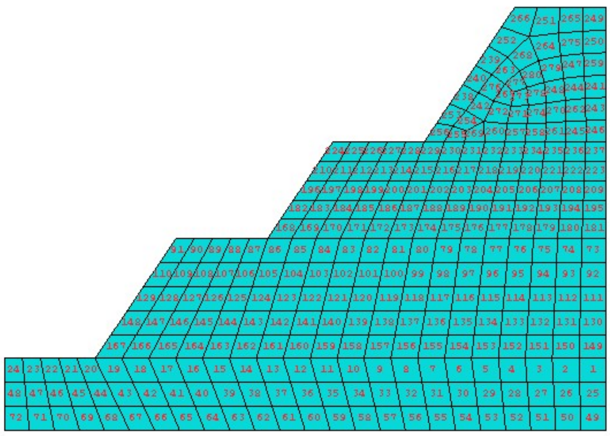

Fig. 4. Finite element model of slope

3.5 Calculation schemes

The slope project is in Luochuan County, Yan'an City. The annual average rainfall is 606 mm, which concentrates in June, July, and August. For numerical simulation, this study hypothesized that annual rainfalls all occurred in June, July, and August, which were once every month and 2 h in each rainfall event. The rainfall intensity in 2 h was constant. In this way, rainfall intensity was calculated to be 101 mm/h. The total operation time was determined to be 5 years to simulate deformation failure laws of cutting loess slope under influences of long-term rainfall. The distribution of rainfall intensity in 5 years based on the abovementioned studies is shown in Fig. 5.

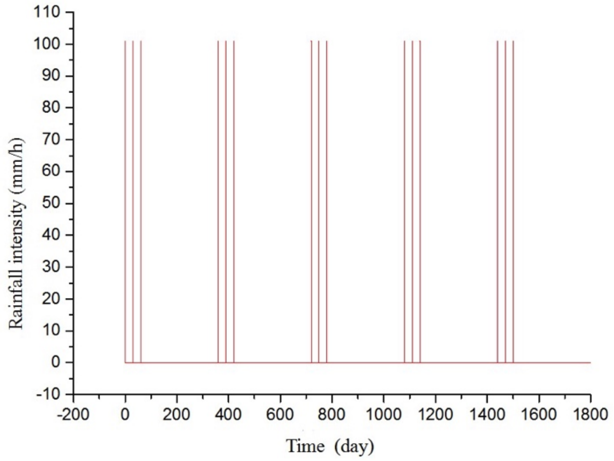

Fig. 5. Variation curves of rainfall intensity

4 Simulation results analysis

4.1 Calculated results of seepage

Based on creep theory of loess in Section 3.1, the secondary developed ABAQUS was used for fluid–solid coupling computation of the slope model in Fig. 4. Pore water pressure distributions in the slope during rainfall and 1 day after the rainfall are shown in Figs. 6 (a) and (b). Clearly, pore water pressure mainly concentrated in slope shoulders during rainfall, especially in the level-1 slope shoulder. This finding might be due to that rainwater infiltrated from the superior-level slope surface concentrated at front lower position and then was discharged. Thus, a saturation belt was formed below the slope shoulder to hinder downward migration of rainwater which was infiltrated from the slope shoulder. Excess pore water pressure was formed temporarily at the slope shoulder. As the rainwater infiltrated from the superior-level slope migrated downward continuously, excess pore water pressure at the lower-level slope shoulder was more obvious than that at the superior-level slope shoulder. The maximum pore water pressure reached 192.2 kPa at the level-1 slope shoulder during rainfall, and it was about 176.2 kPa at the level-2 slope shoulder. However, it was only 128.2 kPa at the level-3 slope shoulder. Obviously, i landslide would inevitably occur at slope shoulder during rainfall due to the excess pore water pressure.

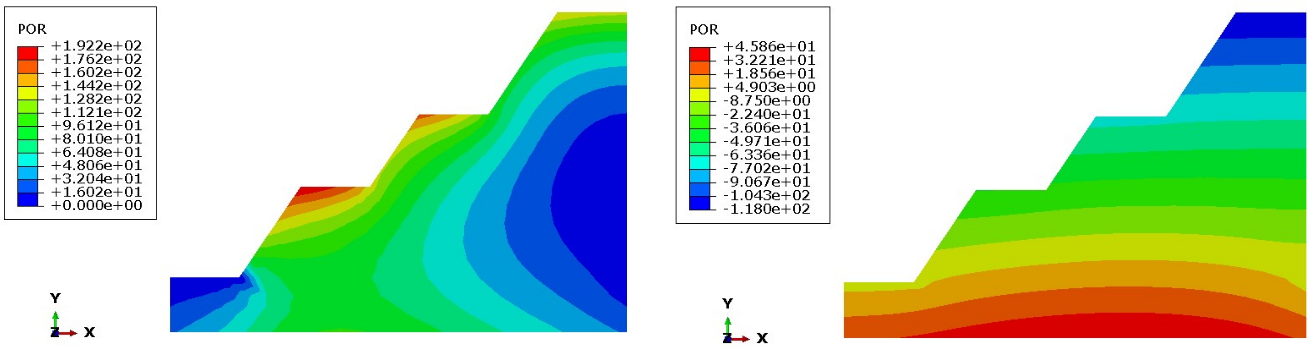

(a) (b)

Fig. 6. Distributions of pore water pressure. (a) Pore water pressure distribution during rainfall. (b) Pore water pressure distribution at 1 day after rainfall

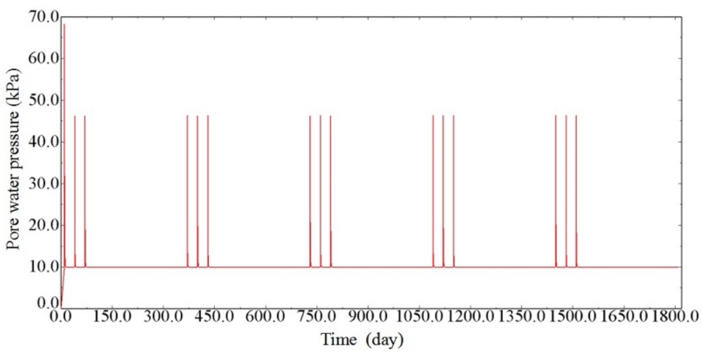

Fig. 7. Variation curves of pore water pressure at 1 m below the level-1 slope foot

Fig. 6 (b) shows that excess pore water pressure formed on the slope surface dissipated quickly after rainfall, and it was dissipated completely at about 2 days after the rainfall. A negative pore water pressure in the slope was observed above the level-1 slope foot, which indicates that it was unsaturated. On contrary, a positive pore water pressure in the slope was found below the level-1 slope foot, and its value had a linear positive relationship with depth. Pore pressure at level-1 slope foot was 0 kPa, which means that the groundwater level formed after rainfall was equal to level-1 slope foot and soil mass below it was saturated. Reasons were analyzed as follows. The infiltrated rainwater migrated downward or be discharged from the slope surface, and soil mass above the level-1 slope foot was dewatered gradually after rainfall and was unsaturated. However, soil mass below the level-slope foot was kept saturated after rainfall because of the lack of discharge channels. Fig. 7 shows that pore water pressure at 1 m below the level-1 slope foot increased to 46 kPa quickly during rainfall, but it dropped quickly to 10.0 kPa after rainfall. This only echoes with local hydrostatic pressure, which implies that soil mass after level-1 slope foot was in the saturated state.

4.2 Calculated results of stress

Shear stress distribution in slope during rainfall is shown in Fig. 8. Clearly, shear stress in slope during rainfall mainly concentrated at slope feet, especially at the level-1 slope foot. Reasons were analyzed as follows. Dead loads of upper soil mass of the slope increased due to rainwater infiltration, which increased greater potential energy of sliding. This phenomenon was mainly offset by shear strength of soil mass at the level-1 slope foot. Thus, a great shear stress was developed at level-1 slope foot. During rainfall, the maximum shear stress reached 63.01 kPa at level-1 slope foot. Some concentration of shear stress was observed at level-2 and level-3 slope feet, but it was not very obvious. The maximum shear stresses at level-2 and level-3 slope feet were only 55.79 kPa. This finding reflects that the potential sliding surface of the slope under influences of rainfall was the pull-type failure which developed upward from level-1 foot through the local site circle. Although relatively great shear force was found at level-1 slope foot, the distribution range was small and it was not connected with upper part. Thus, the slope did not develop overall instability during long-term rainfall conditions.

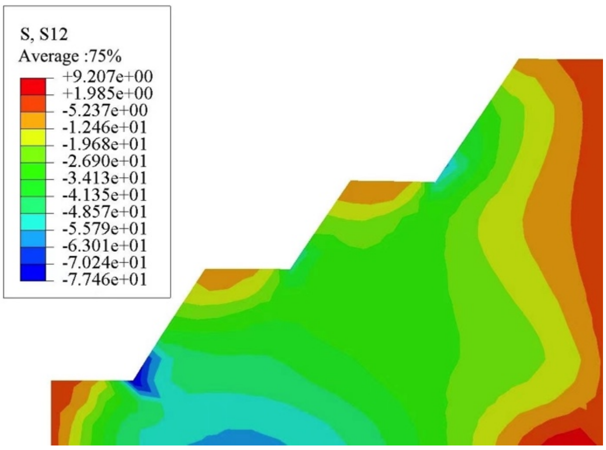

Fig. 8. Shear stress distribution during rainfall

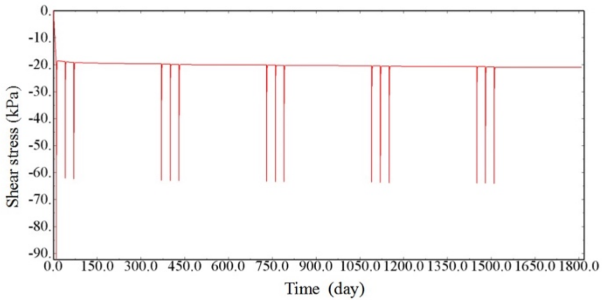

Fig. 9. Variation in shear stress at level-1 foot

The variation in shear stress at level-1 slope foot with time is shown in Fig. 9. Obviously, shear stress at level-1 slope foot increased quickly to about 63 kPa during rainfall, but it dropped to about 20 kPa quickly after rainfall. This result indicates that influences of rainfall on loess slope were elastic. Moreover, shear stress continuity at level-1 slope foot increased slowly as time progressed. It increased from about 18 kPa to about 21 kPa in 5 years. In summary, creep properties of loess brought a slow increase in shear stress at level-1 slope foot and stability of loess slope was degraded slowly as time progressed.

4.3 Calculated results of deformation

Distribution of plastic strain of the loess slope at the end of 5th year is shown in Fig. 10. Clearly, plastic strain of the loess slope mainly concentrated at different levels of slope shoulders during rainfall, especially at the level-1 slope shoulder. This result only agrees with pore water pressure distribution in the slope during rainfall. Excess pore water pressure formed at slope shoulders during rainfall was the major cause of plastic strain, which verifies the statement that landslide has occurred at slope shoulders during rainfall. Landslides at slope shoulders decreased the slope angle at different levels. Thus, rainfall-induced landslide at slope shoulders was called cutting effect of rainfall. Notably, new slope surfaces formed after landslides at different-level slope shoulders were arc-like, which appears to be consistent with Sweden arc method in classical soil mechanics.

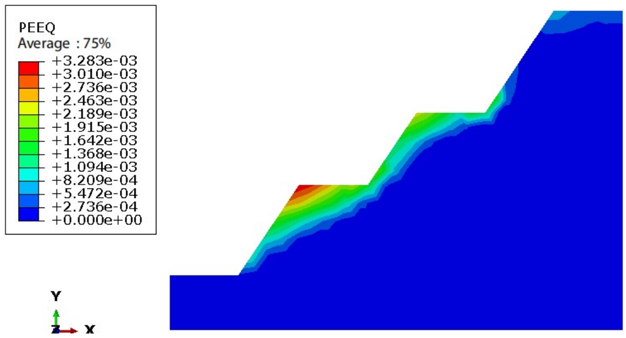

Fig. 10. Plastic strain distribution at the end of 5th years

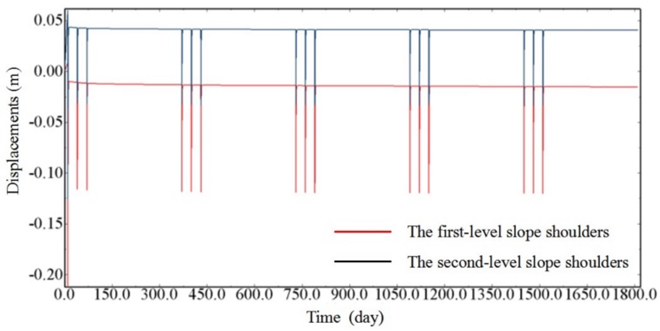

Fig. 11. Variations in horizontal displacements at level-1 and level-2 slope shoulders

The variations in horizontal displacements at the level-1 and level-2 slope shoulders in 5 years are shown in Fig. 11. Similar to variations in shear stress and pore water pressure in the slope, the horizontal displacements at the level-1 and level-2 slope shoulders increased quickly during rainfall. However, they dropped quickly after rainfall, which reflects some elastic deformation characteristics. Horizontal displacements at the level-1 slope shoulder during and after rainfall were significantly greater than those at the level-2 slope. This result also proves that the slope has developed bottom-up pull-type failure. Moreover, the horizontal displacement at the level-1 slope shoulder was a negative, which suggests that rainfall induced forward deformation of the level-1 slope shoulder. However, the horizontal displacement at the level-2 slope shoulder was a positive, which implies the rear softening and settlement of the slope due to rainwater infiltration. Consequently, slope body above the level-2 slope leaned back more than forward deformation. Obviously, slow creep deformation of horizontal displacements at level-1 and level-2 slope shoulders have been developed as time progressed. However, the creep deformation volume was very small. The creep deformation volume at level-1 slope shoulder in 5 years was about 5 mm. Creep rate decreased continuously, and it was stable at the end of the 5th year. This finding demonstrates that influence of creep deformation of loess slope was not obvious, and it was not the major controlling factor of slope stability when the governance scheme was strict.

5. Conclusions

ABAQUS was developed for the secondary time based on Burgers creep model to disclose the creep instability mechanism of cutting loess slope under influences of long-term rainfall. The model was used for fluid–solid coupling analysis on extensively distributed cutting loess slopes in northern Shaanxi Province, China. Variation curves of pore water pressure, plastic strain, and displacement of cutting loess slope under influences of long-term rainfall were obtained. The main conclusions could be drawn as below:

(1) The pore water pressure in cutting loess slope mainly concentrates at slope shoulders during rainfall, especially at the level-1 slope shoulder. It is manifested as excess pore water pressure, which is the major cause of landslides at loess slope.

(2) Large-scaled plastic deformation has occurred at different levels of slope shoulders with the increase in operation period, which decreases slope angles at all levels. This phenomenon proves the shoulder cutting effect of loess slope by rainfall. Consequently, the slope surface is generally arc-like.

(3) Shear stress concentrates at different-level slope feet during rainfall, especially at the level-1 slope foot. In other words, cutting loess slope develops pull-type failure which develops upward gradually from the level-1 slope foot during rainfall.

(4) Shear stress at slope foot and horizontal displacement at different-level slope shoulders develop slow creep laws during rainfall. Moreover, creep rate decreases gradually, and it is stable at the end of the 5th year. This result indicates that creep influences loess slope to a very limited extent.

In a word, the proposed creep instability mechanism of cutting loess slope under influences of long-term rainfall further discloses the instability mode and internal causes of the slope. Moreover, influences of creep on stability development of loess slope are analyzed. Research conclusions can provide some references to study stability development of loess slope. However, the rainfall period in this study is set only 5 years due to the limited article length, which is far shorter than the practical operation period. Longer rainfall period has to be considered in future studies according to practical engineering conditions to obtain more valuable guidelines for loess slope governing projects.

References

1. Li, Y. R., Shi, W. H., Aydin, A., Beroya, M. A., Gao, G. H., "Loess genesis and worldwide distribution". *Earth-Science Reviews*, 201, 2020, pp.102947.
2. Liu, K., Ye, W. J., Jing, H. J., "Shear strength and damage characteristics of compacted expansive soil subjected to wet–dry cycles: a multi-scale study". *Arabian Journal of Geosciences*, 14, 2021, pp.2866.
3. Liu, K., Ye, W. J., Jing, H. J., "Shear strength and microstructure of intact loess subjected to freeze–thaw cycling". *Advances in Materials Science and Engineering*, 2021, pp.1173603.
4. Li, H. B., Feng, Z. X., Ahmed, A. T., Yombah, M., Cui, C. Y., Zhao, G. J., Guo, P., Sheng, Y. P., "Repurposing waste oils into cleaner aged asphalt pavement materials: A critical review". *Journal of Cleaner Production*, DOI:10.1016/j.jclepro.2021.130230
5. Li, H. B., Feng, Z. X., Hua, L., Ahmed, A. T., Zhang, M. M., Zhao, G. J., Guo, P., Sheng, Y. P ., "Performance and inorganic fume emission reduction of desulfurized rubber powderyrene‐butadiene‐styrene composite-modified asphalt and its mixture". *Journal of Cleaner Production*，DOI:10.1016/j.jclepro.2022.132690
6. Zhang, X. Q., Yuan, B., "Analysis and evaluation of the stability of loess slopes in Northwest China". *Coal Technology*, 40(04), 2021, pp.126-128.
7. Ye, W. J., Cui, C.Y., Gao, C., Dong, Q., Jing, H. J., Deng, Y. S., "The influence of hydraulic properties and rainfall patterns on the deformation laws of loess slopes". *Journal of Henan University of Science and Technology*, 42(4), 2021, pp.60-68.
8. Carlini, M., Chelli, A., Francese, R., Giacomelli, S., Giorgi, M., Quagliarini, A., Carpena, A., Tellini, C., "Landslides types controlled by tectonics-induced evolution of valley slopes (Northern Apennines, Italy)". *Landslides*, 15(2), 2018, pp. 283-296.
9. Xie, W. L., Li, P., Zhang, M. S., Cheng, T., Wang, Y., "Collapse behavior and microstructural evolution of loess soils from the Loess Plateau of China". *Journal of Mountain Science*, 15(8), 2018, pp. 1642-1657.
10. Sun, P., Zhang, M., Feng, L., Wang, S., Dang, X. Y., Liu, M. M., "Water sensitivity of loess and its spatial-temporal distribution on the Loess Plateau". *Northwestern Geology*, 52(2), 2019, pp. 117-124.
11. Lian, B., Wang, X., Zhan, H., Wang, J. D., Peng, J. B., Gu, T. F., Zhu, R. S., "Creep mechanical and microstructural insights into the failure mechanism of loess landslides induced by dry-wet cycles in the Heifangtai platform, China". *Engineering Geology*, 300, 2022, pp.106589.
12. Yan, L. J., Lei, T. W., Zhang, J., Zhang, Q. W., Qu, L. Q., "Finite element method for one-dimensional rill erosion simulation on a curved slope". *International Soil and Water Conservation Research*, 3(1), 2015, pp. 28-41.
13. Tang, Y., Wu, W., Yin, K. L., Wang, S., Lei, G. P., "A hydro-mechanical coupled analysis of rainfall induced landslide using a hypoplastic constitutive model". *Computers and Geotechnics*, 112, 2019, pp. 284-292.
14. Lu, Z., Jin, Z., Kotronis, P., "Numerical analysis of slope collapse using SPH and the SIMSAND critical state model". *Journal of Rock Mechanics and Geotechnical Engineering*, 14(1), 2022, pp. 169-179.
15. Chueasamat, A., Hori, T., Saito, H., Sato. T., Kohgo, Y., "Experimental tests of slope failure due to rainfalls using 1g physical slope models". *Soils and Foundations*, 58(2), 2018, pp. 290-305.
16. Kaya, A., Akgün, A., Karaman, K., Bulut, F., "Understanding the mechanism of slope failure on a nearby highway tunnel route by different slope stability analysis methods: a case from NE Turkey". *Bulletin of Engineering Geology and the Environment*, 75(3), 2016, pp.945-958.
17. Cogan, J., Gratchev, I., "A study on the effect of rainfall and slope characteristics on landslide initiation by means of flume tests". *Landslides*, 16(12), 2019, pp. 2369-2379.
18. Acharya, G., Cochrane, T., Davies, T., Bowman, E., "Quantifying and modeling post-failure sediment yields from laboratory-scale soil erosion and shallow landslide experiments with silty loess". *Geomorphology*, 129(1-2), 2011, pp.49-58.
19. Derbyshire, E., Dijkstra, T. A., Smalley I. J., Li, Y., "Failure mechanisms in loess and the effects of moisture content changes on remoulded strength". *Quaternary international*, 24, 1994, pp. 5-15.

20. Chinkulkijniwat, A., Tirametatiparat, T., Supotayan, C., Yubonchit, S., Horpibulsuk, S., Salee, R., Voottipruex, P., "Stability characteristics of shallow landslide triggered by rainfall". *Journal of Mountain Science*, 16(9), 2019, pp. 2171-2183.
21. Schwarber, J. A., Darrow, M. M., Daanen, R. P., Stevens, D., "Loess is more: field investigation and slope stability analysis of the tanana 440 landslide, Interior Alaska". *Environmental and Engineering Geoscience*, 28 (3), 2022, pp. 255-273.
22. Leshchinsky, B., Vahedifard, F., Koo, H. B., Kim, S. H., "Yumokjeong Landslide: an investigation of progressive failure of a hillslope using the finite element method". *Landslides*, 12(5), 2015, pp.997-1005.
23. Cross, M., "Sensitivity analysis of shallow planar landslides in residual soils on south Pennine hillslopes, Derbyshire, UK". *Bulletin of Engineering Geology and the Environment*, 78(3), 2019, pp. 1855-1872.
24. Sadovenko, I. O., Puhach, A. M., Dereviahina, N. I., "Investigation of hydrogeomechanical parameters of loess massifs in conditions of technogenic underflooding and development of technical recommendations for strengthening of bases of foundations". *Journal of Geology, Geography and Geoecology*, 28(1), 2019, pp. 173-179.
25. Chang, J., Song, S., Feng, H., "Analysis of loess slope stability considering cracking and shear failures". *Journal of Failure Analysis and Prevention*, 16(6), 2016, pp. 982-989.
26. Zhu, D. Y., Lee, C. F., Qian, Q. H., Chen, G. R., "A concise algorithm for computing the factor of safety using the Morgenstern Price method". *Canadian Geotechnical Journal*. 42(1), 2005, pp. 272-278.
27. Yi, H., "*Based on the rheological properties of the collapsible loess*". Master thesis of Wuhan University of Technology , China, 2017, pp. 8-11.
28. Niu, Q., "*Secondary development of loess creep model based on FLAC3D and application on time prediction of landslide sliding*". Master thesis of Lanzhou University of Technology, China, 2017, pp. 27-33.